https://doi.org/10.15407/ufm.20.03.502

L.I. KARBIVSKA, V.L. KARBIVSKYY, and A.O. ROMANSKYY
G.V. Kurdyumov Institute for Metal Physics, NAS of Ukraine,
36 Academician Vernadsky Blvd., UA-03142 Kyiv, Ukraine

DETERMINISM OF THE SYMMETRY OF A SINGLE-CRYSTALLINE SURFACE OF INTERFACE AT OBTAINING 0*D*-AND 2*D*-STRUCTUES OF NOBLE METALS AND INDIUM ON SILICON

The review article deals with 'quantum engineering' of growing of silver films on semiconductor substrates that allows obtaining new forms of matter. The results on the energy dispersion of electron states in epitaxial Ag(111) films obtained on Si(001) and Si(111) are presented. The splitting of bands is explained, and analysis of the Shockley's surface states is given. Superstructures, which are formed on the surface of monolayer silver nanostructures, are analysed in detail. A detailed analysis of the energy states of the noble-metal quantum wells is given. The mechanism of formation of a noble-metal nanorelief on the (111) and (110) surfaces of Si single crystal during multistage thermal deposition is investigated. The symmetry of the interface surface of the single-crystal Si(111) 7×7 silicon plane is deterministic in the growth mechanism of the hexagonal-pyramidal structures of copper, silver, and gold. The morphological features of the indium surface during its thermal deposition on the Si(111) and Si(110) surfaces are investigated. The formation of clusters of a regular cubic shape is observed that indicates the formation of In nanocrystals. The formation of In nanoclusters (of ≈10 nm size) on the Si(111) surface and the subsequent modification of the single-crystal surface morphology response in the calculated curves of electron density of states.

Keywords: quantum wells, energy dispersion, noble metals, surface, morphology, scanning tunnelling microscopy, thermal deposition.

1. Introduction

For specialists involved in the study of the growth processes of thin films and the study of the surfaces of materials, the fabrication of metallic nanostructures on the atomic-clean surfaces of semiconductor sin-

gle crystals is one of the most important areas of research. Among other things, it is so because in many electronic devices the metal-semiconductor boundary section is a working component. Many years of intensive research in this direction eloquently prove its importance. Nevertheless, despite that, fundamental research in this area is still interesting and relevant. This topic still attracts a lot of attention, including due to a number of interesting effects associated primarily with preparation technology and size effects.

It is known that the growth modes (regimes) of substances on different substrates can be described by three main types [1]: two-dimensional (2*D*) mode or layer-by-layer growth (Frank–van der Merve growth mode); combined growth mode, which begins as layer-by-layer growth but then proceeds to three-dimensional island growth (Stranski–Krastanov growth mode); three-dimensional island film growth (Volmer–Weber growth mode). When we vary thermodynamic parameters based on the analysis of boundary energy and surface energy, these three growth modes may have differences [2]. The growth of metals on surfaces of semiconductors has heteroepitaxial character. For a long time, it was thought that the growth of metals on semiconductor surfaces obeys the aforementioned growth regimes. However, in 1996, a new approach was published [3]. This approach was based on the critical film thickness during the growth of silver on the GaAs(110) substrate surface. In the aforementioned work, it was shown that with a less critical film thickness, they are uneven, and with increasing thickness, they grow into a smooth, even layer. A new method for growing thin films was proposed when Smith *et al.* [3] applied the two-step method described earlier by Evans *et al.* [4] for growing silver on the surface of GaAs(110) at ≈135 K and further annealing at room temperatures. It was discovered that the initially uneven Ag film consisting of nanoscale 3*D* clusters self-organizes into an atomically flat film, when the system is warmed to room temperature. Moreover, such a transition from cluster organization of the surface to an atomically smooth one can take place only when the total number of layers is no less than six monolayers (ML) [3].

Due to the study of nature of this new type of critical thickness of growth, the 'electronic growth' model was proposed [5]. Electrons in thin films are quantized along the direction of the surface normal and some of these electrons can be scattered at the interface of film substrate. Consequently, as the thickness changes, there will be a change in the electron energy, which includes oscillations of electrons along the normal direction to the surface and electrostatic potential due to the appearance of an electrical double layer with scattered electrons at the interface. The balance between these phenomena determines the thickness at which the total electron energy has a local minimum [5]. Thus, the film tends to align and acquires an atomically flat morphology.

The study of Cu, Ag, and Au nanostructures formation during their thermal deposition on semiconductor single-crystal surfaces provides a valuable information about organization of metallic nanostructures, in particular, metallic single-component ones. In view of that, it is very important from a fundamental point of view. On the other hand, given the applications in electronics for example, they are no less important from a purely practical side. Nowadays, noble metal nanostructures are used in various consumer technologies that use their physical properties, particularly optical, electrically conductive, antibacterial, and others [6–10].

This paper focuses on an overview of the study of the electronic, spectral, morphological, and structural properties of monolayer films of noble metals on the surfaces of single crystals.

2. Energy Dispersion in Ag(111) Epitaxial Films Obtained on Si(001) and Si(111)

The authors of Ref. [11] investigated the dispersion of the quantum-well states (QWS) in Ag(111) epitaxial films grown on Si(001) and on Si(111). The studies were carried out *via* photoelectron spectroscopy with angular resolution (ARPES). It was found that the planar band structure of a thin Ag film is essentially determined by the interface of the substrate (Fig. 1).

The *s* and *p* valence electrons of silver in the film are spatially limited and quantized along the normal to the Ag(111) film. For a bulk metal, the Ag(111) $E(k_{\|})$ is isotropic, but the size of the dispersion becomes significant, if 4*d* states participate in the hybridization with an increase of the binding energy [13, 14]. As established by Müller *et al.* [12], in-plane effective mass $m_{\|}^{*}$ increases with binding energy E_{bind} (the solid line in Fig. 1). Such a tendency of the *s*–*p* band $m_{\|}^{*}$ of bulk Ag is explained by the electron states of quantum wells in the Ag/Cu(111) system [12]. However, this trend does not correspond to the ARPES data for QWS in Ag/Si(001) and Ag/Si(111), which show completely opposite aspirations of $m_{\|}^{*}$ with respect to the binding energy.

The change in plane dispersion can be caused by transverse deformation of film, which is caused by the lattice mismatch of the interface and the film [15]. This deformation effect was theoretically calculated and, as it turned out, it is quite insignificant, and, if there is one, it is homogeneous in the entire energy range. However, this does not explain the results for the QWS in Ag/Si(001) and Ag/Si(111), which are significantly different from bulk Ag. Herewith, the possibility that the lattice deformation changes $m_{\|}^{*}$ cannot be ruled out, thus, affecting the hybridization of the Ag 4*d* and *s*, *p* valence states.

Another factor that was considered in explaining the anomalous plane band dispersion was the small size of the planar coherent region.

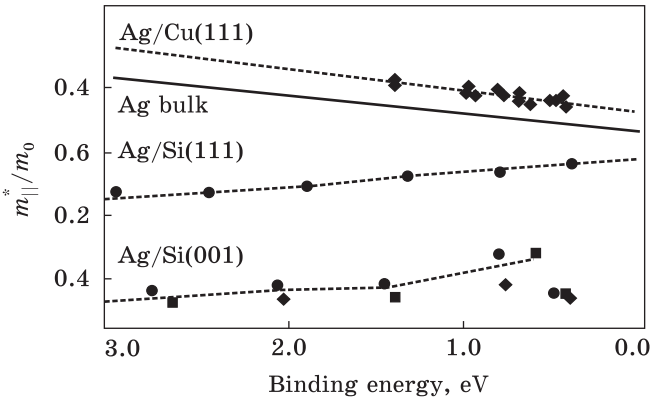

Fig. 1. Ratios of (topological) effective mass ($m^*_{\|}$) to the free electron mass (m_0) as a function of the binding energy of the QWS at $k_{\|} = 0$ for Ag(111) film on Cu(111) [12], Si(111), and Si(001) substrates. The data were obtained at $h\nu$ = = 22.7, 10.3, and 9.3 eV, respectively (–, ●, ■, ♦)

Although this effect of transverse size of film is unlikely, since the Ag(111) film had an area size of less than 200 Å, which was observed with scanning tunnelling microscopy (STM) and low-energy electron diffraction (LEED) [16–19], which goes far beyond the quantum limit <50 Å [20].

During the photoelectron investigation of deposited Ag layers on the V(100) surface, Valla *et al.* [21] observed a large discrepancy between the Ag *s–p* planar band dispersion and the behaviour of free electrons. From the similarity between such an unexpected dispersion of the QWS and that on the V(100) substrate with the 3*d* band, Valla *et al.* [21] suggested a strong hybridization between these two electronic states. Such hybridization with electron states of the substrate can cause unusual dispersions of QWS observed in Ag/Si(001) and Ag/Si(111).

Shaded areas in Fig. 1 correspond to the valence region of the silicon substrate below the maximum of the valence band. When QWS are located within this energy range, they can hybridize with the electron states of the substrate. Apparently, this unusual behaviour of $m^*_{\|}$ in Ag/Si(001) and Ag/Si(111) occurs inside such regions. Note also that the masses $m^*_{\|}$ for Ag/Si(001) and Ag/Si(111) differ little, when the corresponding QWS are located outside the region of the substrate: the QWS with $n = 1$ in Ag/Si(001) has $m^*_{\|} = 0.3m_e$ at $E_{\text{bind}} = 0.5$ eV (Fig. 1). It is assumed that the wave functions of the electrons of the Ag(111) *s–p* band and the Si(001) *s–p* band do not hybridize with each other. It is also not entirely clear how hybridization can affect a planar band dispersion of film with a thickness of 14–16 ML with shielding values inside the metal [22, 23]. A correct theoretical description with necessity required knowledge of the band structure of Ag films on monocrystalline silicon substrates.

Another unusual aspect of the planar dispersion of QWS is the fact that the QWS with $n = 2$ in Ag/Si(001) splits into two subbands with significant dispersion (Fig. 2). Such a splitting is less likely to occur

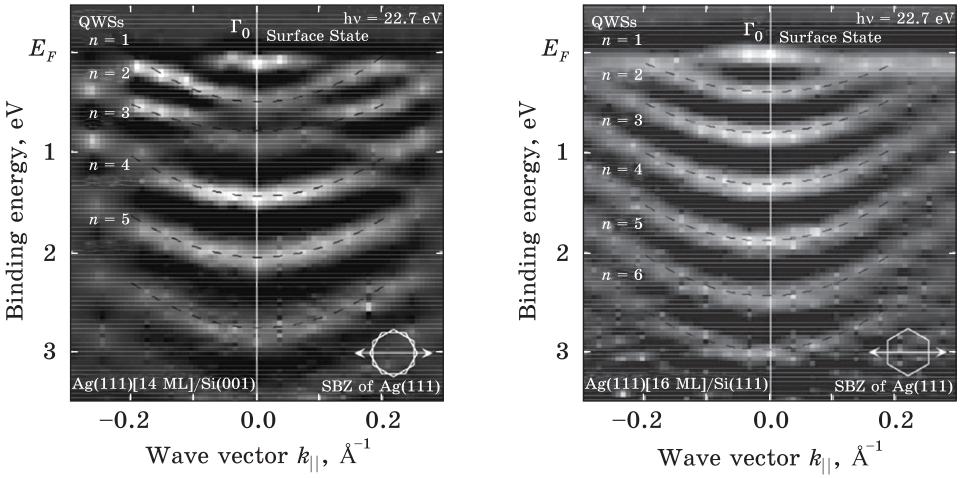

Fig. 2. Binding energy E_{bind} *vs.* wave vector $k_{||}$ for 14 ML thick Ag(111) film on Si(001) substrate along the [101] axis of the substrate ($h\nu$ = 22.7 eV) [11]

Fig. 3. The same as in the previous figure, but for 16 ML film on Si(111) substrate [11]

with large quantum numbers, *e.g.*, n = 3. Analysing the splitted bands, it is necessary to analyse in detail the possibility of the influence of photoemission from the surface of the substrate itself. The STM and electron diffraction results [17, 18] show that Ag(111) films uniformly cover the substrate surface, while the mean free path for the corresponding photoelectrons is no more than ≈10 Å [24], which is about one third of film thickness Ag(111). It can be assumed that splitting can be caused due to contributions from different parts of the silver film, which have different thickness. However, this explanation is also not plausible, as it was shown that silver films are homogeneous with a height variation of ±1 or ±2 ML and the expected energy splitting for such variations in height is much less than the observed one [25, 26]. The parabolic dispersion law should describe the expected dispersion of the QWS from slightly different film thicknesses. Such splittings were observed for the Ag(111) films on Si(001) with different thicknesses.

The authors of [11] proposed an explanation of such a splitting of QWS within the framework of the quantization rule of the phase shift. It has been established that the difference in the phase shift between the inner and outer side of the valence band of the substrate corresponds to 0.3π, which, with using theoretical calculations, gives the difference between the split E_{bind} branches for QWS with n = 2 equal to 0.10 ± 0.04 eV. This ratio agrees quite well with the observed energy splitting at 0.13 ± 0.03 eV for QWS with n = 2 (Fig. 2). Similar calculations were performed for QWS with n = 3 and 4 in accordance with the observed energy splittings, *e.g.*, 0.13–0.18 eV for n = 3. These calcula-

tions confirm the idea of a phase break at the substrate edge during emission not normal. However, such a model is not sufficiently complete to describe in detail dispersion of the split QWS.

If we apply such theoretical calculations for the Ag/Si(111) system, the change of the binding energy of QWS near the edge of the bulk Si band at $E_{\text{bind}} \approx 0.5$ eV [QWS with $n = 1$ in Ag/Si(111)] will be around 0.03 ± 0.03 eV. Such a small value is determined by flattening of the s–p band of silver close to the top of the band (Fig. 3).

3. Shockley's Surface States

The Shockley's surface electron states on silver epitaxial films grown on a Si(111)7×7 surface were studied in the work of Neuhold *et al.* [16]. The films were obtained by a two-step method [3]. The LEED method showed that, before the annealing, only blurred spots were observed, and after that, distinct hexagons were revealed (Fig. 4).

If we consider a silver layer as a quantum well with valence electrons, the wave vectors of stationary states in the well have the values, which are described *via* the equation $k_z = n\pi/Na + C$, where a — atomic-layer width, N — the number of atomic layers in the metal film, n — principal quantum number. Amendment C occurs due to the finite height of the walls forming the pit. This value can be found theoretically and vary very slightly in a certain energy range [27, 28]. Therefore, this equation describes the quantization condition for the k values, which, due to the monotony of the band structure, lead to discrete energy levels, first observed by means of the photoelectron spectroscopy by Wachs *et al.* [29].

Figure 4 [30] compares the spectra of Ag(111)/Si(111)7×7

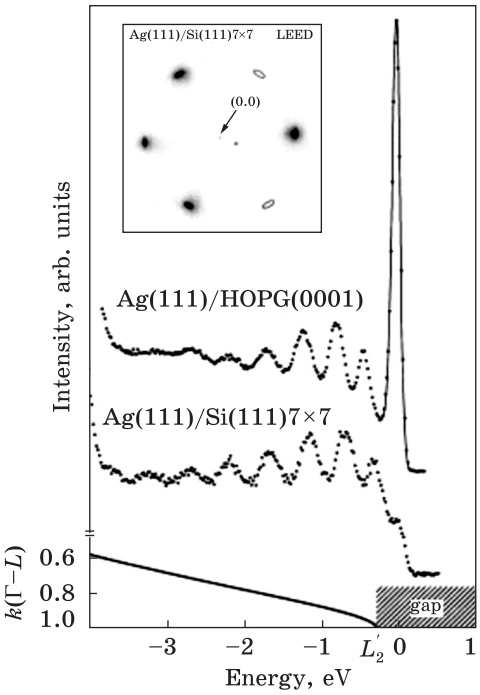

Fig. 4. Comparison of photoelectron spectra obtained with excitation photon energy of 47 eV and emission normal to ≈50 Å thick Ag(111) on the HOPG and Si(111)7×7. The diagram below shows the characteristic part of the Ag band structure near the L point (L_2' — edge of the band). The wave vector is taken as the radius vector of the Brillouin zone along the Γ–L direction. The insert in the figure shows the LEED of the Ag(111) film on Si(111)7×7 [30]

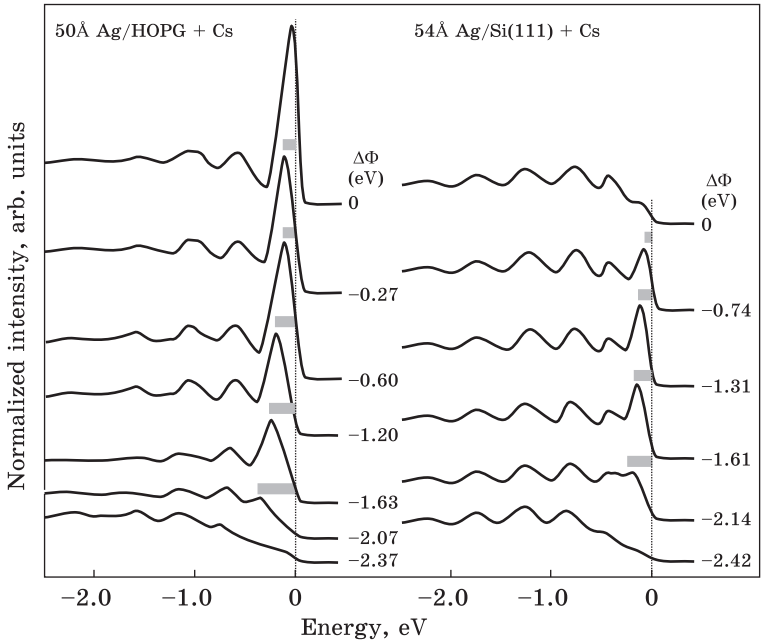

Fig. 5. Photoelectron spectra of Ag films on HOPG (left) and Si(111) (right) substrates coated with Cs submonolayer. Vertical bars indicate shift of peaks ($\hbar\omega$ = = 47 eV) [27]

and Ag(111)/HOPG(0001) systems (here, HOPG abbreviates the highly oriented pyrolytic graphite) obtained by photoelectron spectroscopy at a temperature of 130 K (the substrate temperature during Ag deposition).

In the band gap along the Γ–L direction (the shaded area below Fig. 4), there are Shockley's surface states, which give a peak near the Fermi energy E_F in the Ag/HOPG spectrum in Fig. 4. Its energy is 50 meV below E_F at the temperature of 130 K [31]. It is noteworthy that the peak is absent in the spectrum of the Ag(111)/Si(111)7×7 system obtained in a similar way. The so-called phase accumulation model was used to explain the differences in the spectra (Fig. 4). In this model, the surface states are stationary states in a one-dimensional (1D) quantum well containing a potential barrier from the vacuum side and a band gap of the crystal on the other side [32]. Quantum-mechanical solutions are in the form of phase shifts in the reflection of the wave functions of electrons from these barriers [27, 28]. It is easy to show that the energy of the Shockley's surface state, which is the lowest proper state of this well, depends on the height of the vacuum barrier, that is, on the work function [27], and on the energies of the band edges [31]. An experimental evaluation of the dependence of the energy of surface states on the

work-function magnitude was made. The use of the adsorption of the alkali-metal submonolayer leads to a significant decrease in the work function. The effect of reducing the work function and its effect on the experimental spectra of surface states is shown in Fig. 5.

The upper left curve (in Fig. 5) for the Ag(111) surface contains peaks and significant emission of surface states near E_F. As an amount of precipitated Cs increases, a decrease in the work function is observed. Such behaviour was previously observed for Cs/Cu(111) and Na/Cu(111) in Refs. [33, 34]. The decrease of the intensity of the peaks of surface states with the deposition of Cs occurs due to the redistribution of its charge in the energy-momentum space [35]. The unperturbed electron wave function can be detected in a limited region, and when surface states cross the edge of the L_2' band at the level of 0.3 eV below E_F, their wave function spreads into the bulk, and the electrons corresponding to this state will have less sensitivity to surface photoemission.

In order to quantify the shift of the energy of surface states with a change in the work function, the peaks of the surface states of the quantum well were modelled using the Voigt peaks described by the Fermi function with experimentally determined parameters. On the left in Fig. 6, the results of this analysis for Ag(111) spectra on HOPG are shown by circles.

Given solid line reflects the energies of surface states taken from the phase accumulation model, in which the effect of adsorption of Cs is assumed to lead to a change in the work function [27]. One can see that a simple model describes well the behaviour of surface states.

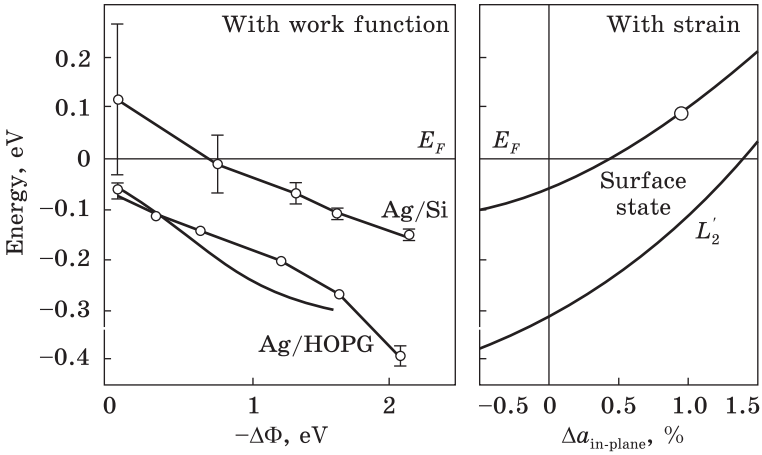

Fig. 6. Shift of the surface states with changes of the work function and strain. On the left, the energies of the surface states (from Fig. 5) are compared with the energies of the phase accumulation model (solid line). On the right, there are calculated energies of the L_2' edge of s–p band. The circle marks the point on the theoretical curve, where the energy of the surface states is shifted by 150 meV relative to the equilibrium value, as it is the case in Ag(111)/Si(111) 7×7 [31]

In Figure 5 to the right, we can see the results of the effect of Cs adsorption on the x-ray photoelectron spectra of the 54 Å thick Ag(111) film obtained on Si(111). The upper curve reflects the spectrum of the clean surface. Figure 4 shows only the peaks of the quantum well in the s–p band. No signal from surface states was found in the vicinity of the Fermi edge. Nevertheless, with a decrease in the work function (Φ) upon the adsorption of Cs, an increase in the intensity of the peak below E_F occurs. This peak is the most pronounced in the spectrum of the work function change $\Delta\Phi = -1.31$ eV. With a subsequent decrease in the work function, the intensity of this peak decreases. After its first manifestation at $\Delta\Phi = -0.74$ eV, the energy of its maximum decreases with decreasing work function. Thus, the emission from the surface states of the Ag(111) layers obtained on Si(111)7×7 is due to the shift of the surface states to the unoccupied region. The downward shift caused by adsorption of Cs causes an intersection with the Fermi level. The energies of the surface states obtained from the spectra are shown in Fig. 6. In order to model the spectra for the clean surface of the Ag(111)/Si system with a similar restrictive parameter obtained in the case of the Ag(111)/HOPG system, it is necessary to have a surface state almost 120 meV above E_F. The surface states of the Ag(111)/Si(111)7×7 system shift, on average, by 150 meV relative to the states in the Ag(111)/HOPG system. This value is sufficient to empty completely the surface states of the clean Ag(111) surface at a given temperature [31].

Consequently, several effects can cause a shift in surface states. In thin epitaxial Ag layers, the surface states of Ag(111) demonstrate significant shifts, which are explained in terms of the interaction of the weakly damped wave function of the surface state in the substrate [36]. The film thickness of about 50 Å, which was used in the work [16], was much longer than the attenuation length ≈28 Å [37], which makes this explanation of the above observations impossible.

The lateral localization of the wave function of the surface state on the tops of the islands, which was considered in Ref. [20], is equally unlikely, since the island size necessary to obtain a noticeable shift is much less than the lateral coherence length of LEED. Since the Ag/Si(111)7×7 interface boundary has significant distinctive parameters [38], this should lead to the disappearance of LEED. The LEED spots (Fig. 4) demonstrate that the localization of the surface states of Ag(111) cannot make a significant contribution to the observed energy shift.

The effect of band edges on the energy of the surface state is a direct explanation of the shift of the surface state in Ag/Si(111)7×7. Due to its close proximity, the lower band edge (L_2') has a huge impact. Therefore, it is reasonable to assume that this quantity determines the observed shift. This view is supported by the fact that the highest peak of the quantum well, corresponding to the principal quantum number

$n = N - 1$, has a higher energy in Ag/Si(111) than in Ag/HOPG. Since the number of Ag layers is *ca* 21 in both cases, this peak should occupy the same position relative to the edge of the band. This means the observed energy difference indicates a shift in the edge of the L_2' band. Nevertheless, variation of the correction coefficient C in equation $k_z = n\pi/Na + C$ (see designations above) for Ag films on two substrates may affect the energy positions of the QWS.

Since deformation is a widespread characteristic of film growth on substrates with lattice mismatch and was observed on epitaxial silver films of the same thickness [39], its effect on the L_2' energy should be considered. The Ag band structure for deformed (stressed) lattices was calculated through the empirical pseudopotential method (EMP) in Ref. [40]. The described scheme is sufficient to describe the properties of a simple band structure of Ag s–p electrons. In order to reproduce the experimental value of –0.3 eV for the energy L_2' [41] in an unstressed lattice, the bands after the calculation were shifted by 225 meV. Since the L_2' value is determined using the EMP, the energy of the surface state is derived from the phase accumulation model. This scheme can be verified by using the temperature dependence of the energy of the surface state, as made by Paniago *et al.* [31]. The temperature expansion coefficient relates the sample temperature to the isotropic deformation of the silver lattice. If we use the value $19 \cdot 10^{-6}$ K^{-1} [42], then using the described procedure, we obtain the value 0.12 meV/K for the shift of the surface state depending on temperature. This result well agrees with the experimentally determined value of 0.17 meV/K obtained in Ref. [31]. The deviation may be due to the narrowing of the band gap L with lattice vibrations that was calculated by Larsson and Pendry [43].

It is assumed that the stress that exerts pressure on the lattice and accompanies the process of forming epitaxial Ag(111) films changes the lattice constant of the (111) plane. As a result, the lattice constant of the plane perpendicular to this one also changes. During deformation, the volume of the crystal will be maintained. This condition was used in calculations when describing lattice deformation. In the right part of Fig. 6, the results of a theoretical review are shown. The calculated energy of the surface state is already strongly shifted at low tensile stresses in the (111) plane (compressed along the [111] direction). In order to explain the observed shift of 150 meV, the Ag(111) lattice grown epitaxially on Si(111) must be deformed by approximately 0.95%. A tensile stress of this magnitude observed in silver films of comparable thickness on MgF_2, Si(100) and mica [39] was attributed to the polycrystalline growth of Volmer–Weber. It was suggested that its nature belongs to the relaxation of grain boundaries and the effects of recrystallization in a silver layer. Increased recrystallization due to the subsequent annealing stage should lead to a further increase in the tensile

stress. In addition, the lattice order is improved, as evidenced by LEED spots, and the surface is levelled that is a necessary condition for observing QWS in the s–p band (Figs. 4 and 5). Differences in the temperature expansion of silicon and silver cannot contribute to the deformation presented in this system, since the deposition and measurement were carried out at the same temperature. Due to the limited attenuation length of 28 Å [37], the energy of the surface state during deformation changes only for the uppermost layers of film.

Silver layers obtained in a similar way on GaAs(110) substrates also show quantum-mechanical peaks indicating uniform growth morphology, but with no surface states. In Ref. [3], using scanning tunnelling microscopy, it was shown that the surface state is absent on the Ag(111) structure. However, there are data for which the deformation is a controversial issue.

Jiang *et al.* [44] described the procedure of measurements of both the surface structure and electronic properties of thin silver films. Using scanning tunnelling spectroscopy (STS), thin Ag films grown on a GaAs(110) substrate and obtained by a two-step method were studied [3]. The STS method allows us to study unoccupied electron states on the surface of films, which are above the Fermi level, in contrast to the photoelectron-spectroscopy method used earlier, in which the range of recorded energies is limited to the Fermi level.

The STS spectra, which show the dependence $(dI/dV)/(I/V)_{\text{mean}}$ of the voltage V, are shown in Fig. 7. All spectra have three significant peaks in the density of states. Two of them are associated with occupied ($V < 0$) electronic states and one with unoccupied (V positive) state. The peaks that are observed below E_F, *i.e.*, associated with the occupied states, change with a change in the film thickness, although the peak of free electronic state did not respond to the film thickness. The occupied states can be associated with QWS that appeared under the restriction on z of the Ag film, while the unoccupied states are the Shockley's surface states (energetically, they occupy the positions at the level of ≈180 meV).

The authors of Ref. [44] used the quantization condition for the wave vector of stationary QWS given above to determine the k_z value. Using the data in Fig. 7, the authors plotted the dependence of the energy levels (peaks in Fig. 7) on the film thickness (Fig. 8).

Analysis of the energy positions of the QWS and the thickness of films allows one to derive the s–p band dispersion in thin Ag films. The principal quantum number n in the first Brillouin zone must be between 1 and N (N is the number of atomic layers). Therefore, the first occupied state below E_F corresponds to the QWS with $n = N - 1$ and the wave vector will be $k_z = (N - 1)\pi/Na$. The wave vector at the boundary of the Brillouin zone (point L) is then reads as $k_{zL} = \pi/a - k_z = \pi/Na$. By anal-

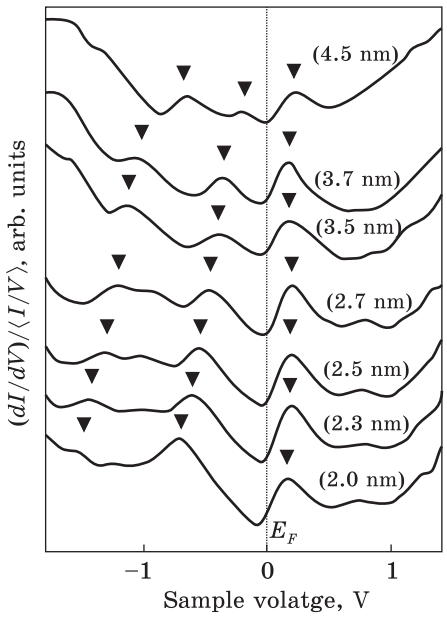

← *Fig. 7.* STS spectra of Ag films with thicknesses of 2.0–4.5 nm [45]

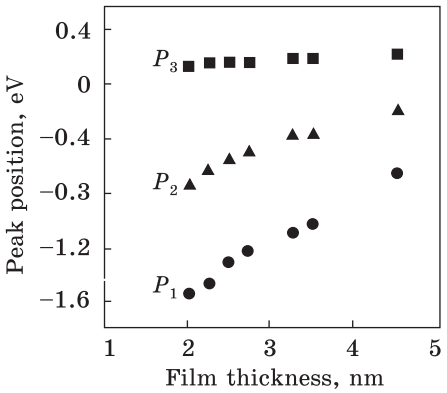

Fig. 8. Energy positions of the STS spectra peaks *vs.* the film thickness [44]

ogy, for the wave vector of the neighbouring state, the formula will be as follows: $k_{zL} = 2\pi/Na$.

Figure 9 shows the band structure along the direction of Γ–L. The solid line describes the band structure of bulk silver. Around point L, the data behaves similarly to pure Ag(111) (solid line). Nevertheless, the experimentally observed energy values shifted upward by 190 ± 20 meV relative to theoretical values. With increasing distance from point L, they deviate more significantly towards higher energies. Thus, the dispersion and the width of the band of thin Ag films on GaAs(110) substrates are smaller than those are known for the theoretical band structure of pure Ag.

During the construction of the experimental data of the band structure, the correction C in the above-mentioned equation for k_z was not taken into account that is associated with the influence of the interfaces. Indeed, on the one hand, the amendment would introduce a horizontal shift, but would in no way affect the energy shift, since, around point L, the energy states are above the maximum of s–p band for pure Ag(111) (Fig. 9). On the other hand, the phase shift at the Ag–vacuum interface changes very little with a change in thickness and the contribution to the band structure of this interface is insignificant [4, 16]. In this case, E_F lies at the level of the band gap of GaAs on the side of the Ag–GaAs interface. Therefore, electrons with energies close to E_F should be Bragg reflected from this interface and the phase shift should be approximately π.

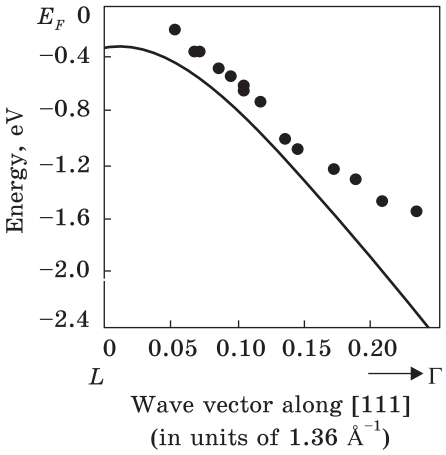

Fig. 9. The *s–p* band structure of the Ag film near the point *L* along the Γ–*L*. The circles show the energy states for QWS obtained *via* the STS method [44]

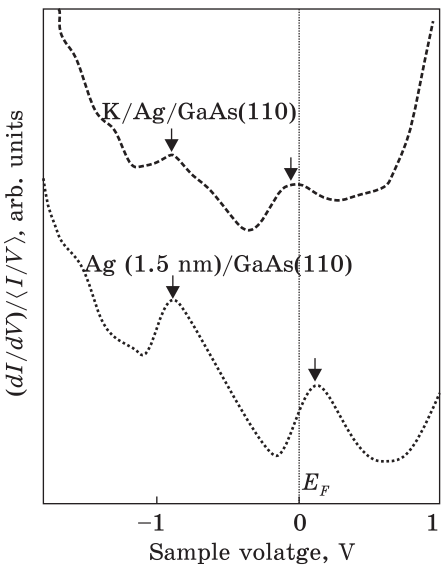

Fig. 10. The STS spectra obtained for clean surface of 1.5 nm thick Ag film on GaAs(110) and after deposition of 0.2 nm of K on the Ag film surface [44]

For a detailed analysis of the surface states, the authors of [44] deposed potassium on the surface and compared the STS spectra. As Figure 10 shows, after the deposition of potassium, energy of free states decreases by ≈190 meV, and these states are occupied. Deposition did not affect the occupied states. This potassium deposition effect can be explained, taking into account the fact that potassium reduces the work function of the sample. At the basis of the phase accumulation model, Shockley's states are shifted to lower energies due to a decrease in the vacuum barrier, *i.e.* the work function. The ≈190 meV shift for Shockley's states should be due to the decrease of the work function by 1.2 eV [16]. Similar shifts for Shockley's states, with a decrease in the work function, were also observed for Ag films grown on Si(111) surfaces [16] and on surfaces of other noble metals [33, 34]. This experiment confirms the assumption that the main observed maximum in the free states belongs to the Shockley's surface state.

In Figure 10, potassium deposition does not change the QWS positions, although lowering the work function should increase the length of the QWS wave function tails deep into the barrier in the direction of vacuum. According to rough estimates, a decrease in the work function of 1.2 eV leads to a change in the wave vector of first quantum-well state only by $\Delta k_{z(n=N-1)} < 0.05$ nm^{-1} that corresponds to the energy shift of the QWS less than 20 meV. Such a small shift cannot be resolved in measurements at the room temperature.

After analyzing the energy positions of the surface states of the bulk (111), Jiang *et al.* [44] concluded that the surface states of thin Ag films on the GaAs(110) surface are shifted upwardly by 210 ± 30 meV. This shift in magnitude is comparable to the shift observed for the dispersion of the *s*–*p* band.

The energy shifts of the *s*–*p* band as well as a significant decrease in the width of the band during film dispersion as compared to the bulk material may be due to the lattice stress in thin films. It was shown that an increase in the temperature of noble metal crystals causes a shift of the band structure upward toward E_F [31, 46] due to a temperature increase in the lattice constant at high temperatures. An increase in the lattice causes a decrease in the overlap of the wave functions, reducing the width of the band. Using the results of calculations based on the empirical pseudopotential method (EPM), the authors of [44] estimated that a shift of about 200 meV corresponds to a planar tensile strain $\Delta a \approx 1\%$. Ag thin film on GaAs(110) has a superstructure. The appearance of the superstructure confirms that the film is stressed. The LEED studies also confirm the presence of deformation. Therefore, [111] orientation of the Ag film is deviated by approximately 4° in accordance with the orientation [110] of the GaAs substrate [47, 48]. If we assume that the Ag–GaAs interface has the same slope, we can assume an Ag film as (667)-oriented film with (111) microfaces. In such a structure, the distance between two steps on the Ag(667) surface is 3.16 nm that is greater about 2 times than the average distance (1.5 nm) between the bands of the quasi-periodic modulated surface [49]. In such a structure, unrelaxed Ag(667) films should have a large lattice mismatch of approximately 6% as compared with the GaAs(110) lattice along the [001] direction. It is likely that the lattice mismatch partially weakens the quasi-periodic superstructure, which leads to an internal lattice stress. The authors of [44] observed identical quasi-periodic superstructures in all Ag films, regardless of their thickness. In this connection, at a stress in a thin film, an upward shift of the electron *s*–*p* band occurs.

Thus, the upward shift of surface states can be associated with the upward shift of the electron *s*–*p* band and the effect of lattice stress. In the model of the phase approach, Shockley's states occupy the lowest state in the potential well limited by the potential barrier from the vacuum side and the band gap of the crystal from the other side. The energy of Shockley's states depends on the work function as well as on the position of the edge of the band gap (point *L*). In this case, the last shifts upward by 190 ± 20 meV in comparison to the energy band structure of the bulk material of f.c.c. Ag(111) at *L* point.

Jiang *et al.* [44] proved why other unoccupied states did not arise for the QWS. The *s*–*p* band of electrons of f.c.c. Ag has a wide band gap of 4.2 eV along the Γ–*L* direction near the point *L* [50]. The range of

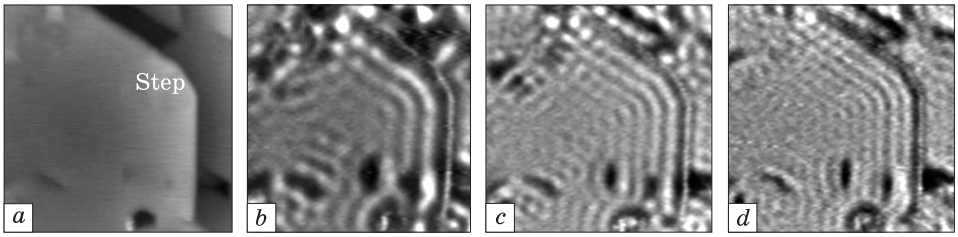

Fig. 11. STM (*a*) and dI/dV (*b*)–(*d*) images (31.5×31.5 nm^2) for 20 ML thick Ag(111) film, where the bias voltages V_S is 0.35 V (*a*), 0.15 V (*b*), 0.25 V (*c*), and 0.35 V (*d*) [51]

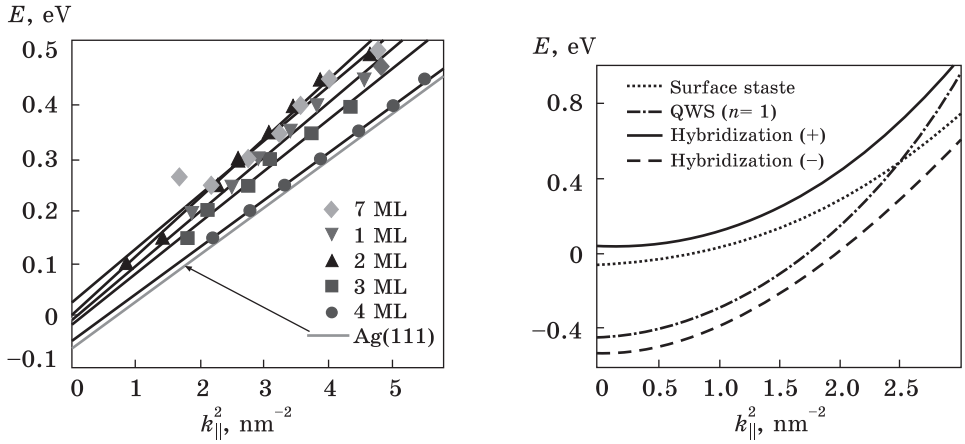

Fig. 12. Dispersion graphs of the surface states for the films of different thicknesses and for bulk Ag [51] (see also Ref. [3] in [51])

Fig. 13. Changing of the dispersion of the surface-state band because of the hybridization with n = 1 QWS [51]

voltages applied to the sample from 0 to 1.5 V was within the energy limits of the band gap. Therefore, there could be no free QWS states along the Γ–L direction. The electron energy in this direction does not increase, but increases along the lateral directions (Γ–X and Γ–W).

A group of Japanese scientists in the paper of Sawa *et al.* [51] studied the thickness-dependent behaviour of Shockley's surface states. They were interested in the question-challenge, due to what the upward shift of the bottom of the surface dispersion band occurs with a decrease in the thickness of the Ag film. The dI/dV graphs show the standing waves of surface electrons that appear at the edges of the steps, the monolayer well and partial dislocations (Fig. 11). Using these images, the wavelength of the surface electron was found. In the calculations, the distance between the peaks of standing waves in the region distant from the defects and dislocations was used in order not to take into account the various quantum limitations of the electrons in these narrow sur-

face regions. With the determination of the wavelength λ, the plane wave vector $k_{\parallel} = 2\pi/\lambda$ was actually computed. Having found the surface electron energy E (equals to bias voltage V_s), the authors of the work were able to construct the dependence $E(k_{\parallel}^2)$ plotted in Fig. 12. From this figure, several consequences were concluded. First, surface states have a parabolic dispersion. Secondly, a 40 ML thick film has dispersion close to the dispersion of the surface states of bulk Ag(111). Thirdly, the energy shifts upward with decreasing film thickness (for energies with $k_{\parallel} = 0$, the shift is 77 meV for a film with a thickness of 40 ML, while 77 + 26 meV for a 7 ML thick film).

The fact of the shift of the bottom of the surface-state band E_0 due to the hybridization of the latter with the valence band of the substrate was refuted. For the Si(111) substrate, the valence band maximum is at the level of –0.3 eV below the Fermi level, and the bottom of the surface state band E_0 for the bulk Ag is only at the level of –63 meV, consequently, the energy levels do not overlap, and thus, hybridization is impossible. Although, *e.g.*, for Ge(111) substrates, it is impossible to say so clearly, since the maximum of the valence band in this case is very close to the Fermi level.

The fact of hybridization of the surface state band with QWS inside the film was also refuted. One can observe in Fig. 13 the dispersion of the surface band (dashed line) and the QWS with $n = 1$ (dash-dotted line). These two states intersect at $k_{\parallel} = 2.51$ nm^{-1}. However, degeneration at the intersection begins and the two states are split into upper and lower branches when the hybridization interaction $H_{SQ} = \langle \text{QWS}|V|SS\rangle$ is introduced between the surface state and the QWS with $n = 1$ at their intersection [51, 52], which are indicated in this figure as solid and dashed lines. The exact H_{SQ} value is unknown in the presented system. Although, as reported, H_{SQ} lies in the range from 20 to 180 meV in Bi/Ag films on a Si(111) substrate [51, 52]. Thus, in this study, the variance of split branches was calculated with $H_{SQ} = 100$ and 200 meV.

The theoretical and experimental data on E_0 and the plane effective mass m^* are given in Table below.

The thickness dependence of the theoretically and experimentally found E_0 and m^* values for surface band and QWS film with $n = 1$

Number of Ag ML	E_0 QWS ($n = 1$), eV	Crossing, nm^{-1}	Experiment		$H_{SQ} = 100$ meV		$H_{SQ} = 200$ meV	
			E_0, meV	m^*/m_0	E_0, meV	m^*/m_0	E_0, meV	m^*/m_0
7	–1.08	4.07	26	0.37	–54	0.42	–27	0.41
10	–0.83	3.54	–6	0.37	–52	0.41	–18	0.40
20	–0.45	2.51	0	0.34	–52	0.38	–19	0.36
30	–0.38	2.26	–11	0.39	–53	0.37	28	0.35
40	–0.31	2.01	–51	0.42	–49	0.34	46	0.34

Due to hybridization, it is assumed that E_0 moves downward and m^* becomes larger with decreasing thickness. However, in the experiment, inverse dependences on thickness were observed (the 4-th and 5-th columns in Table). Therefore, it was excluded from consideration about the hybridization of the surface state and QWS as the cause of the observed shift of the surface states of the Ag(111) films. This calculation indicates that H_{SQ} is very small, and no significant splitting occurred in the presented Ag/Si(111) system.

Sawa *et al.* considered the change in the electronic structure of Ag films caused by stress [16]. The lattice constant for Ag is 25% less than for Si. The calculation using the EPM demonstrated that the plane tensile strain shifts E_0 upward on the surface of the Ag(111) film [16].

Indeed, as the film thickness increases, the misfit stress gradually weakens in the heteroepitaxial system [53]. From this point of view, it is reasonable to assume that E_0 shifts upward, since the thickness of the Ag film decreases, since a decrease in thickness increases the flat tensile strain. This explanation also agrees with the results of the previous study using photoelectron spectroscopy of the temperature-dependent shift E_0 on the surfaces of bulk Ag(111) [31]. Application of the method of photoelectron spectroscopy shows that the shift upward of E_0 at the temperature increase is observable. The same effect is observed due to the stress.

In addition, the calculation with the usage of the EPM indicates that 0.95% of the value of flat tensile stress causes E_0 to be shifted upward by 150 meV [16]. This result confirms that the accumulated stress in the film was not 25%, even for an Ag film with a thickness of 7 ML on the Si(111) substrate. STM studies showed that Ag films contain many dislocations even at a very early stage of the growth [54]. That is why the authors of Ref. [51] interpreted the small shift E_0 by stress relaxation.

4. Quasi-Periodic Superstructures of Ag on Single-Crystal Surfaces

The appearance of the superstructure, which is formed by an Ag film deposited on a GaAs(110) surface, has been studied by Ebert *et al.* [49]. They found that 1*D* quasi-crystals acting as a quasi-periodic self-similar superstructure are formed on the film. The nature of defects changing the surface superstructure of film is also ascertained.

The 1*D* quasi-periodic structure is observed in the formation of thin Ag layers with a thickness of 1.5–1.7 nm using the two-step method [3]. All Ag films exhibit 1*D* modulation in height leading to bands with 0.05 nm grooves on STM images (Fig. 14).

Figure 14 demonstrates that the bands are clear, not having the same separation, and do not form an explicit periodic superstructure.

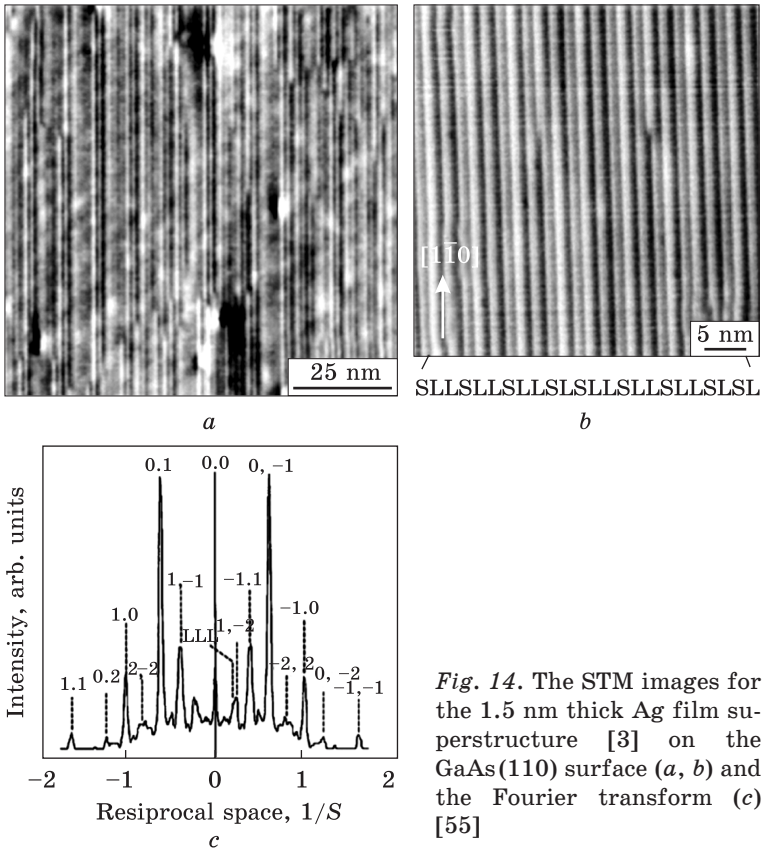

Fig. 14. The STM images for the 1.5 nm thick Ag film superstructure [3] on the GaAs(110) surface (*a*, *b*) and the Fourier transform (*c*) [55]

Two different basic separation intervals with distances between the bands of about 1.2 ± 0.2 and 1.7 ± 0.2 nm can be distinguished (Fig. 14, *b*). The authors identified them with short (S) and long (L) sections, respectively. Figure 14, *a* shows that at low magnifications STM images show bands similar to those in Fig. 14, *b*. Nevertheless, in Fig. 14, *a*, there are significantly longer distances between the bands than in the case of two base bands. Large-size bands arise due to additional height modulation, which overlaps with base-height modulation, resulting in L and S regions. Figure 14, *c* shows the Fourier transform of the bands. The peaks in the Fourier transform are well described and numbered [55] in the basis of two basic elements whose lengths are related to each other according to the principle of the golden section in inverse space. Peaks beyond 1/S are associated with the substructure of the bands and they exhibit properties, which are described by the golden section principle (peak 1.6/S). Due to the Fourier transform as well as spatial images, it was found that the ratio of the long band-separating interval to the short on the STM images is 1.55 ± 0.15. This

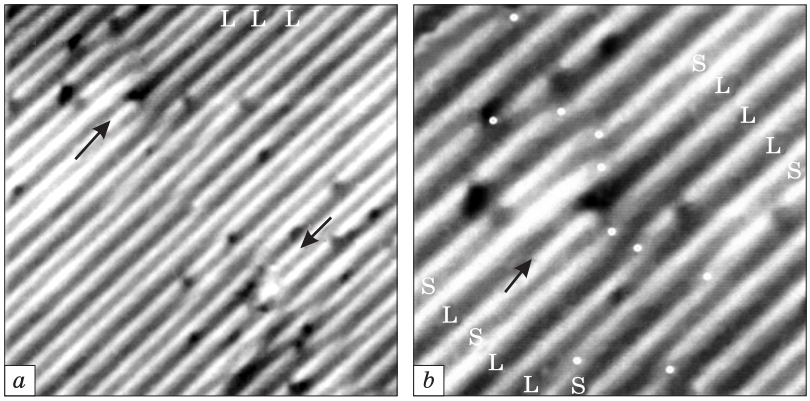

Fig. 15. STM images (with different scales) of the LLL sequence and dislocation correcting this sequence [55]

ratio is consistent within the framework of errors with the ratio of two consecutive members of the Fibonacci sequence for large values of their numbers (F_n, F_{n+1} are sequence members, $F_{n+1}/F_n = \varphi$, where $\varphi = (1+\sqrt{5})/2$ equal to 1.618... is golden ratio). Self-similarity and Fourier transform do not contradict the quasi-periodic type of order.

The bands form a sequence of long and short sections. Such a sequence is indicated in the lower part of Fig. 14, *b*. A large number of such sequences were analysed (with lengths up to 135 areas and a total number of areas over 1500 taken from different Ag films) in order to determine statistically the structural model, which best fits the experimental observations.

Comparison with the Fibonacci sequence shows that the experimentally observed data best fit the sequence of the Fibonacci golden section, since it has the least number of irrelevant sequences. The best observed in the experiment is described by a quasi-periodic golden section sequence with a coherence length of approximately 12.5 nm. This conclusion is also consistent with the LEED data, which can be well explained with taking into account quasi-periodic ordering of the golden section. It cannot be excluded that such a structure can be described using a high-order approximating sequence. However, high-order approximating sequences and quasi-periodic structures differ little, and recognition at this level is beyond the limits of the statistical accuracy under consideration.

The limited coherence length indicates that defects must be present in the sequences. It has been detected that the main defect is the frequent absence of a short section. This one leads to three, and sometimes even more consecutive, long sections. The importance of this type of defect is confirmed by observation of dislocations that correct these sequences from three long sections on the LLSL sequence. It has been

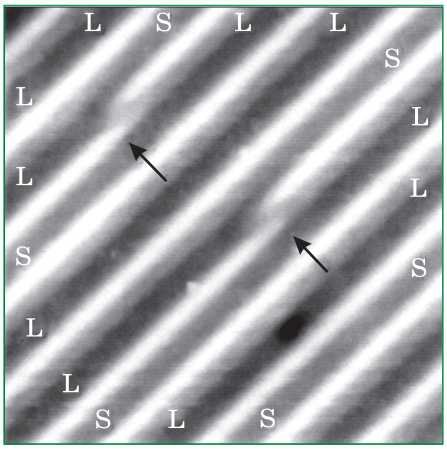

Fig. 16. STM image of Ag film surface with a phason defect [55]

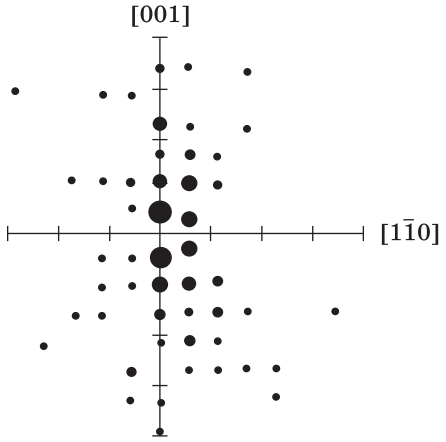

Fig. 17. Distribution of phason defects close to the dislocation cores

shown that the sequences defined by dislocations have much better agreement with the Fibonacci sequence. The coherence length of the corrected sequences increases to almost 11 regions or 17 nm. The number of L regions decreases from 66% to 62% when adjusted, providing a very good agreement with that for the ideal Fibonacci sequence (≈61.8%). Thus, the missing short sections are main defects.

Three consecutive long intervals between areas are labelled as LLL. In the position indicated by the arrow, one additional strip is inserted, which shows a short separation interval with the adjacent strip (section S), *i.e.* the dislocation generates a short section. It was found that such properties were observed with a concentration of approximately $5 \cdot 10^{10}$ cm^{-2}. Each observed dislocation has a Burgers vector oriented parallel to the quasi-periodic direction ([001] direction of the GaAs(110) substrate) with a short separation interval length. A pair of dislocations with opposite Burgers vectors was observed frequently, as shown in Fig. 15, *a*; however, isolated dislocations were observed as well. In Figure 15, *a*, we can see an STM image of such a LLL defect, which can be referred to as a domain wall or as a grain boundary.

In addition to dislocations, there are still other defects responsible for a limited coherence length. Figure 16 shows the most common ones—phason defects. A large degree of disorder occurs due to phason defects. Phase defects by definition are a local displacement of one position of a quasi-periodic lattice to another neighbouring position, violating the quasi-periodic structure. Surface phason defects in Fig. 16 were observed with a concentration of *circa* 10^{12} cm^{-2} [55].

A significant part of phason defects is not uniformly distributed over the surface. Small light circles in Fig. 15, *b* show that phason de-

fects arise close to the core of the dislocation. The STM image indicates that phason defects propagate mainly along the [001] direction from the dislocation core. A statistical analysis of the distribution of phason defects close to the dislocation cores is represented in Fig. 17 [55]. The size of the points in Fig. 17 is proportional to the number of phason defects (within the range of 1–8) per area unit around 14 dislocations. One division along the axes in Fig. 17 corresponds to a length of 3 nm; the centre of coordinates coincides with the core of the dislocation; the strip inserted during dislocation is located on the left side of the x-axis [55].

The authors of Ref. [49] found that all the band shifts due to phason defects occur in the direction opposite to the dislocation core. Thus, dislocations cause oriented phason defects. The appearance of phason defects can be explained from the point of stress relieving; they are close to the core of the dislocation, since phason defects increase the size of the interband interval that is necessary when an additional band is added-on during dislocation. In this case, the static stress field around dislocations is a source of phason defects, whereas early work on icosahedral quasi-crystals reported that the appearance of phason and disorder is associated with dislocation movements [56, 57].

5. Morphological Features of Nanostructures of Noble Metals and In during Their Thermal Deposition on the Si Single Crystal Surfaces

The studies of surface nanorelief were performed on a JSPM-4610 tunnelling microscope (JEOL, Japan). The working vacuum quality during the experiment was such that the pressure was $\leq 10^{-8}$ Pa. Plates of silicon Si(111) and Si(110) single crystal with a size of $7 \times 1 \times 0.3$ mm^3 were used. Preparation of single crystal surfaces was performed by standard methods. Initially, a current of ≈ 0.2 A was conducted through the silicon plate for one day. In this way, the sample was heated up to ≈ 250 °C. After that, the current conducting through the sample raised to 3.0 A being maintaining for 30 s, which corresponded to the sample temperature of about 950 °C. Then, the sample was cooled, after which the (111) and (110) surfaces were imaged *via* a tunnelling microscope (Fig. 18). All studies on a tunnelling microscope were performed in the dc regime.

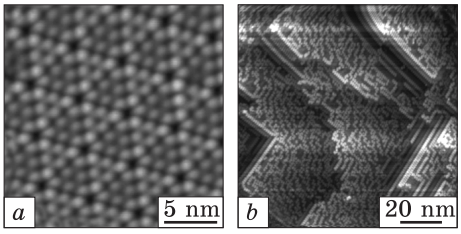

Fig. 18. STM images of the Si single-crystal surfaces: Si(111) (*a*) and Si(110) (*b*) [58]

Gold, silver, copper, and indium were deposed on the surfaces prepared by the thermal evaporation method. As an evaporator, we used a spiral tungsten cuvette containing a metal sample; the cuvette occupied the middle of a metal cylinder with a hole of 3 mm. The distance between the sample and the evaporator was ≈7 cm. The deposition occurred at a current of ≈5.0 A through a tungsten coil, which corresponded to the temperature of ≈100 °C above the melting point of the metal. The time of deposition was about 1–3 s. The deposition of metal on a single crystal surface was performed without heating or cooling the sample. Tunnel spectra were studied using a high-vacuum tunnel spectrometer with atomic resolution of the company JEOL (Japan).

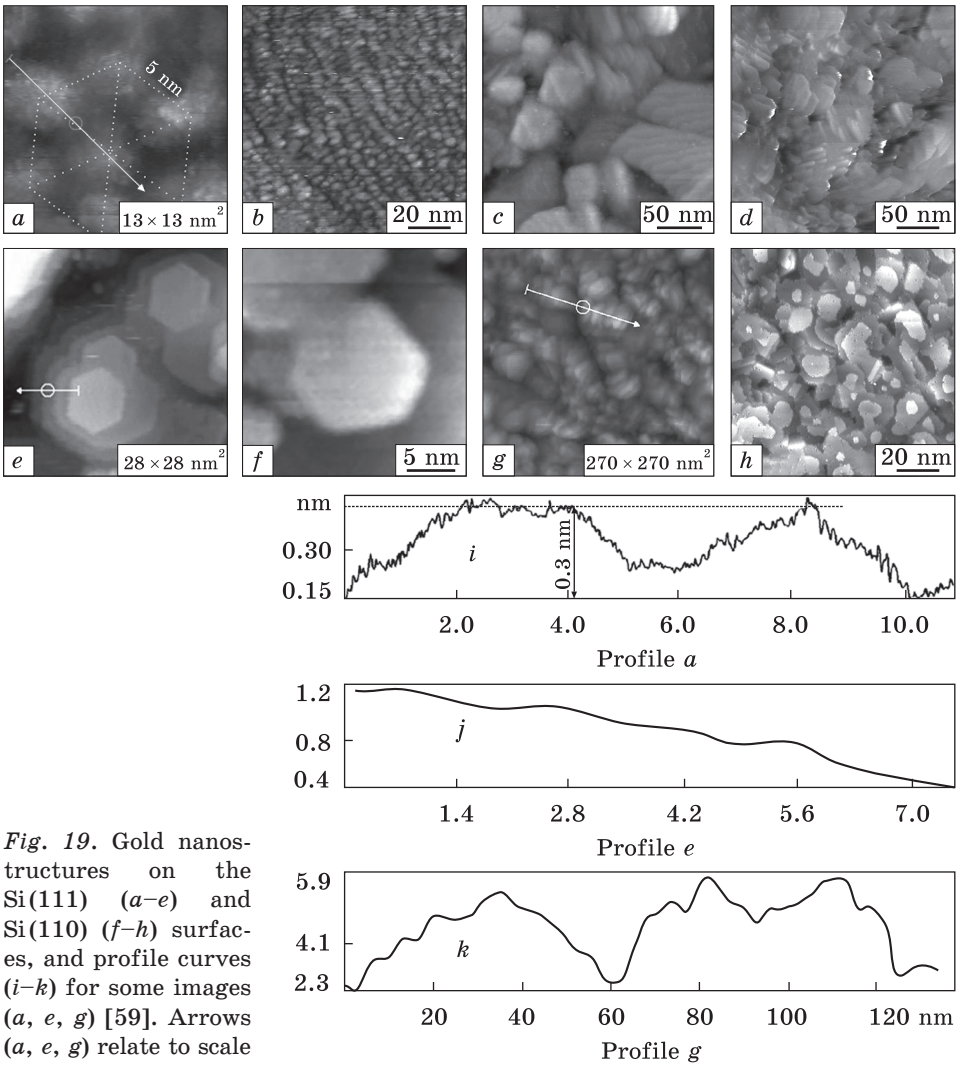

Fig. 19. Gold nanostructures on the Si(111) (*a*–*e*) and Si(110) (*f*–*h*) surfaces, and profile curves (*i*–*k*) for some images (*a*, *e*, *g*) [59]. Arrows (*a*, *e*, *g*) relate to scale

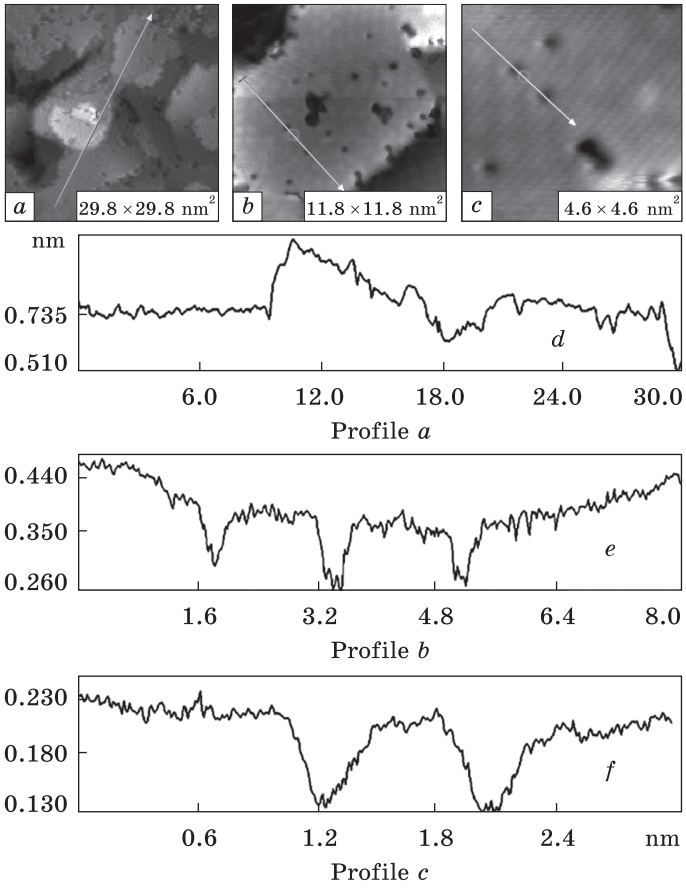

Fig. 20. Flakes of gold on the Si(111) surface (*a*–*c*), where the arrows indicate a scale, and corresponding profiles (*d*–*f*) [59]

Noble metal nanostructures (Fig. 19) can be obtained by varying deposition parameters [58–61]: the deposition time, the distance from the cuvette to the sample, the pressure in the chamber, the melting temperature of the cuvette, or the cooling of the sample.

Using the developed technology, we can obtain hexagonal clusters with a hexagon side of ≈5 nm (Fig. 19, *a*). The geometry of such structures is close to that of the Si(111) 7 × 7 single crystal surface (Fig. 18). Figure 19, *b* shows the chain ordering of clusters. Under certain technological conditions, we obtained 'fractal' leaf-like gold nanostructures (Fig. 19, *c*). Needle-like crystals (Fig. 19, *d*) can be grown under the longer deposition times (≈1 min). The study showed that the stable hexagonal-pyramidal structures of gold could be obtained only on the Si(111) plane. Meanwhile, on the Si(110) plane, we obtained the structures shown in Fig. 19, *f*, which are characterized by the presence of hexagons

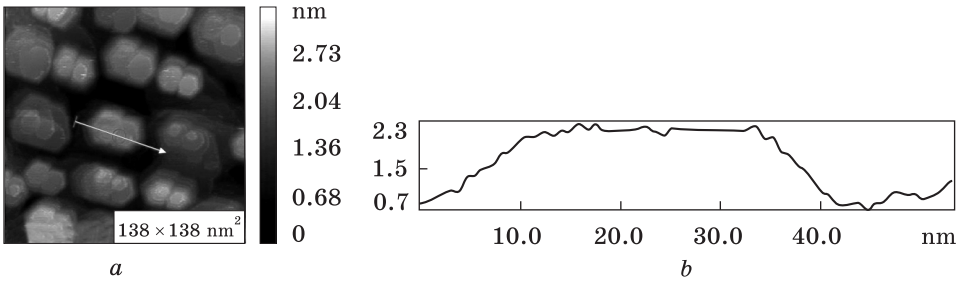

Fig. 21. Pattern of copper nanostructures on the Si(111) surface: 2*D* diagram (*a*) and height curve (*b*). White arrow (*a*) relates to scale

without the formation of pyramids. For short deposition times and vacuum up to 10^{-6} Pa, we observed clusters with a small size distribution (6–8 nm). In this case, an increase of the time of deposition led to the formation of cluster conglomerates (Fig. 19, *g*).

Currently, the investigation and production of monolayer metallic coatings in a higher vacuum is of the significant interest. Combining some methodical and technological characteristics, we reached such a deposition regime, which allowed us to obtain monolayer flake-like gold formations (Fig. 19, *h*). There are areas within the flakes not filled with atoms. After the spectral analysis using the tunnel spectroscopy, we revealed that electron states in these vacancies might possess specific features. Particularly, they can be quantized according to the quantum dots principle.

The parameters of flake shown in Fig. 20. Earlier in [59], we suggested that free sagging flake edges might be possible. However, an adequate answer to this question one can provide by the 3*D*-microscopy only. The case of free existence of a metal monolayer (or its edges in this case) contradicts the solid-state physics general canons.

Analysing vacancies (with diameter of ≈0.5 nm), we noticed that Au atoms are absent in amount of ≈1–3 atoms (Fig. 20, *b*).

Similar situation was observed for Cu deposited with the same technological parameters as Au; the behaviour of formed nanostructures is very close to the morphological features for gold described above. Hexagonal-pyramidal nanostructures of copper are shown in Fig. 21.

Thus, self-ordered hexagonal-pyramidal nanostructures are formed on Si(111) by thermal evaporation of both Cu and Au. The ordering is characterized by parallelism of the corresponding sides of the bipyramid as well as their respective orientation relative to the sides of the 7×7 hexagon of the structure of silicon.

The heights of the bipyramidal formations belong to the range 1–1.5 nm, as can be seen from the vector profiles. The thickness of growth of steps is of ≈0.15 nm that corresponds to the size of an atom. Observed ‘texturing’ in all the figures indicates that all bipyramids

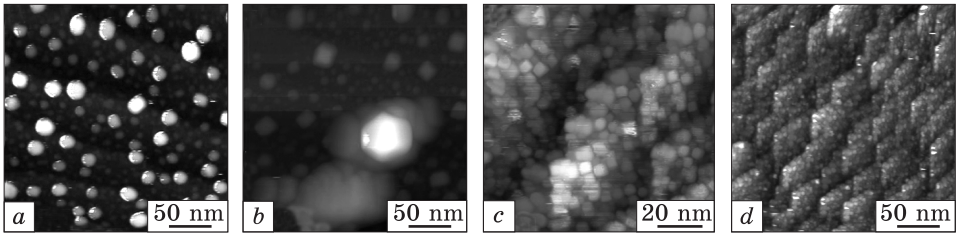

Fig. 22. Indium nanostructures on the Si(111) surface

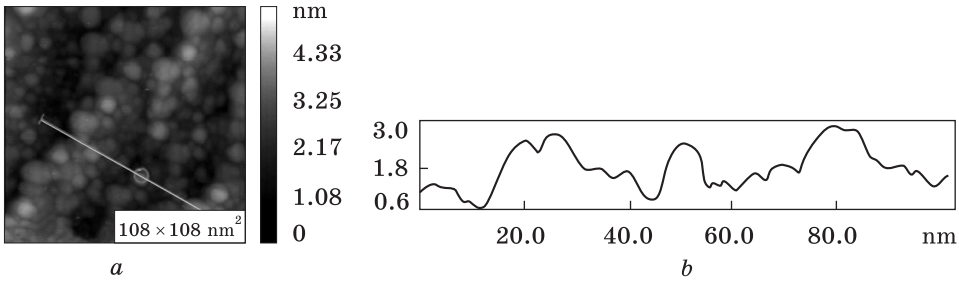

Fig. 23. Profile of indium roughness on the Si(111) surface: 2*D* diagram (*a*) and height curve (*b*)

have the same orientation with respect to the interface structure of the base. Therefore, the symmetry of the interface plane is crucial in obtaining such ordered nanostructures.

The observed growth of steps corresponds to atomic planes. The characteristic distance from the beginning of the plane to the next one is (as is in the case of Au) ≈3 nm [58, 59]. For Cu as well as for Au atoms, it is energetically more advantageous to begin formation of the next plane from this distance. In the case of copper deposition on the (110) surface of a single Si crystal, the observed pattern of nanorelief is similar to the image obtained for Au deposition. Copper, like gold, does not form pyramidal nanostructures on the Si(110) surface (Fig. 19, *f*).

Mentioned above may indicate that the deposition of the atomic Au and Cu gases is partially, but not completely, described by traditional schemes for the nanorelief formation. The dynamic image of a steady flow of atoms is defined by the difference between the flows to and from the surface. Varying the technological parameters of deposition [58–61], we can obtain one or another morphological pattern of the noble metal surface.

In the case of the indium deposition on the (111) and (110) surfaces of the Si single crystals, a completely different mechanism of formation of nanostructures is realized (Fig. 22). The formation of predominantly spherical In clusters is observed on short deposition times (1–3 s). In addition, clusters close to hexagonal or rectangular shape may

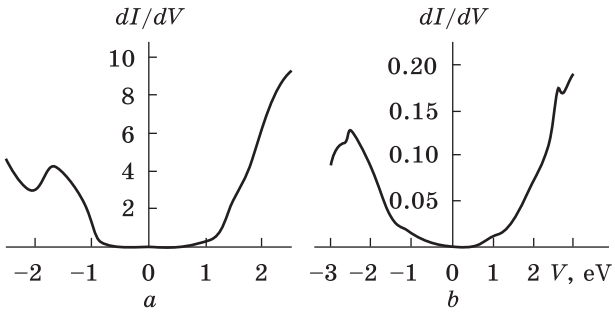

Fig. 24. Densities of electronic states corresponding to images in Figs. 22, *a* (*a*) and *d* (*b*)

be observed (Fig. 22, *a*). The formation of hexagonal clusters on the surface of shapeless cluster (Fig. 22, *b*) was observed when the deposition time was increased up to 5 s. Furthermore, one can see the positioning of rectangular and square clusters. The formation of clusters of correct symmetry unambiguously indicates the formation of indium nanocrystals.

Indium has a much lower melting point (156.6 °C) as compared to gold and copper. Under the same technological parameters of deposition as for gold and copper, we obtained molten indium, which is many times overheated. Its deposition onto the uncooled surface of silicon single crystal resulted to formation of the clusters of form mentioned above.

When the deposition time was increased above 5 s, it led to the formation of the bunch of clusters of predominantly cubic form (Fig. 22, *c*). An average side size of such cubic formations: 4–5 nm.

It is noteworthy that this type of samples has the profile of irregularities with a height of 0.6–3 nm (Fig. 23). There is also a periodic relief substructure in the form of line bunches (Fig. 22, *d*).

Figure 24 shows the tunnel spectra for the two samples. Curve in Fig. 24, *a* demonstrates the density of electronic states (DOS) for image in Fig. 22, *a*. A certain band gap at the Fermi level indicates a nonmetallic character of the cluster, which attributes to ≈10 nm size clusters of In. Figure 24, *b* shows modification of the DOS caused by the surface morphology completely filled with bunches of clusters. The DOS curve is much closer to that of indium in the metallic phase. The first peaks in the region of occupied states characterize the *p* states of indium. For a single cluster, they are localized at ≈1.8 eV and have a narrow peak. But this maximum has a practically non-zero value in the region of zero binding energies, shifts to the region of high binding energies upon transition to the coating. The same tendencies of the DOS curve changing have been observed for the region of free states.

6. Summary

'Quantum engineering' of the silver films growing on semiconductor substrates allows obtaining new forms of the matter. Analysis of the growth of ultrathin metal films convinces that quantum mechanics plays an important role in the design of atomically flat metal layers.

The results on the energy dispersion of electronic states in epitaxial Ag(111) films obtained on Si(001) and Si(111) surfaces are presented. Splitting of energy bands is explained; analysis of the Shockley's surface states is given. Superstructures, which are formed on the surface of monolayer silver nanostructures, are analysed in detail. A detailed analysis of the energy states of the noble metal quantum wells is given.

The mechanism of formation of a nanorelief of a noble metal on the (111) and (110) surfaces of a Si single crystal during multi-stage thermal deposition is investigated. The symmetry of the interface surface of the Si(111) 7×7 plane acts as a determinant factor in the growth mechanism of the hexagonal-pyramidal structures of Cu, Ag, and Au.

The In surface morphological features on the Si(111) and Si(110) surfaces investigated upon the thermal deposition. The regular cubic-shape cluster patterns are observed that indicates the indium nanocrystals formation. The density of electron states varies when the case of a separate ≈10 nm-size In clusters on the Si(111) changes into the case of bunch coating of the single crystal surface (coating thickness no more than 30–40 nm).

REFERENCES

1. H. Liu, Y.F. Zhang, D.Y. Wang, M.H. Pan, J.F. Jia, and Q.K. Xue, *Surf. Sci.*, **571**: 5 (2004). https://doi.org/10.1016/j.susc.2004.08.011
2. E. Bauer, *Z. Kristallogr.*, **110**: 372 (1958). https://doi.org/10.1524/zkri.1958.110.1-6.372
3. A.R. Smith, K.-J. Chao, Q. Niu, and C.-K. Shih, *Science*, **273**: 226 (1996). https://doi.org/10.1126/science.273.5272.226
4. D.A. Evans, M.Alonso, R. Cimino, and K. Horn, *Phys. Rev. Lett.*, **70**: 3483 (1993). https://doi.org/10.1103/PhysRevLett.70.3483
5. Z.Y. Zhang, Q. Niu, C.-K. Shih, *Phys. Rev. Lett.*, **80**: 5381 (1998). https://doi.org/10.1103/PhysRevLett.80.5381
6. G. Yang, Y. Zhou, H. Long, Y. Li, and Y. Yang, *Thin Solid Films*, **515**: 7926 (2007). https://doi.org/10.1016/j.tsf.2007.03.027
7. M. Rai, A. Yadav, and A. Gade, *Biotech. Adv.*, **27**: 76 (2009). https://doi.org/10.1016/j.biotechadv.2008.09.002
8. R.M. Tilaki, A. Irajizad, and S.M. Mahdavi, *Appl. Phys. A*, **84**: 215 (2006). https://doi.org/10.1007/s00339-006-3604-2
9. G. Yang, D. Guan, W. Wang, W. Wu, and Z. Chen, *Optical Mater.*, **25**: 439 (2004). https://doi.org/10.1016/j.optmat.2003.11.002
10. H.-J. Lee, S.-Y. Yeo, and S.-H. Jeong, *J. Mat. Sci.*, **38**: 2199 (2003). https://doi.org/10.1023/A:1023736416361

11. I. Matsuda and H.W. Yeom, *J. Electron Spectrosc. Relat. Phenom.*, **126**: 101 (2002). https://doi.org/10.1016/S0368-2048(02)00145-7
12. M.A. Müller, T. Miller, and T.-C. Chiang, *Phys. Rev. B*, **41**: 5214 (1990). https://doi.org/10.1103/PhysRevB.41.5214
13. H. Wern, R. Courths, G. Leschik, and S. Hufner, *Z. Phys. B*, **60**: 293 (1985). https://doi.org/10.1007/BF01304449
14. H. Erschbaumer, A.J. Freeman, C.L. Fu, and R. Podloucky, *Surf. Sci.*, **243**: 317 (1991). https://doi.org/10.1016/0039-6028(91)90369-4
15. E. Bauer and J. van der Merwe, *Phys. Rev. B*, **33**: 3657 (1986). https://doi.org/10.1103/PhysRevB.33.3657
16. G. Neuhold and K. Horn, *Phys. Rev. Lett.*, **78**: 1327 (1997). https://doi.org/10.1103/PhysRevLett.78.1327
17. M.H.-v. Hoegen, T. Schmidt, M. Henzler, G. Meyer, D. Winau, and K.H. Rieder, *Phys. Rev. B*, **52**: 10764 (1995). https://doi.org/10.1103/PhysRevB.52.10764
18. M.H.-v. Hoegen, T. Schmidt, M. Henzler, G. Meyer, D. Winau, and K.H. Rieder, *Surf. Sci.*, **331–333**: 575 (1995). https://doi.org/10.1016/0039-6028-(95)00320-7
19. G. Meyer and K.H. Rieder, *Appl. Phys. Lett.*, **64**: 3560 (1994); idem, *Surf. Sci.*, **331–333**: 600 (1995). https://doi.org/10.1063/1.111197, https://doi.org/10.1016/0039-6028(95)00325-8
20. R. Fischer, Th. Fauster, and W. Steinmann, *Phys. Rev. B*, **48**: 15496 (1993). https://doi.org/10.1103/PhysRevB.48.15496
21. T. Valla, P. Pervan, M. Milun, A. B. Hayden, and D.P. Woddruff, *Phys. Rev. B*, **54**: 11786 (1996). https://doi.org/10.1103/PhysRevB.54.11786
22. A. Zangwill, *Physics at Surfaces* (Cambridge University Press: 1988). https://doi.org/10.1017/CBO9780511622564
23. H. Luth, *Surface and Interfaces of Solid Materials* (Berlin: Springer: 1995). https://doi.org/10.1007/978-3-662-03132-2
24. S. Hufner, *Photoelectron Spectroscopy, Springer Series in Solid-State Sciences. Springer Series. Vol. 82* (Berlin: Springer: 1995). https://doi.org/10.1007/978-3-662-03150-6
25. J.J. Paggel, T. Miller, and T.-C. Chiang, *Phys. Rev. B*, **61**: 1804 (2000). https://doi.org/10.1103/PhysRevB.61.1804
26. J.J. Paggel, T. Miller, and T.-C. Chiang, *Science*, **283**: 1709 (1999). https://doi.org/10.1126/science.283.5408.1709
27. N.V. Smith, *Phys. Rev. B*, **32**: 3549 (1985). https://doi.org/10.1103/PhysRevB.32.3549
28. N.V. Smith, N.B. Brookes, Y. Chang, and P.D. Johnson, *Phys. Rev. B*, **49**: 332 (1994). https://doi.org/10.1103/PhysRevB.49.332
29. A.L. Wachs, A.P. Shapiro, T.C. Hsieh, and T.-C. Chiang, *Phys. Rev. B*, **33**: 1460 (1986). https://doi.org/10.1103/PhysRevB.33.1460
30. F. Patthey and W.-D. Schneider, *Phys. Rev. B*, **50**: 17560 (1994). https://doi.org/10.1103/PhysRevB.50.17560
31. P. Paniago, R. Matzdorf, G. Meister, and A. Goldmann, *Surf. Sci.*, **336**: 113 (1995). https://doi.org/10.1016/0039-6028(94)00740
32. P.M. Echenique and J.B. Pendry, *J. Phys. C*, **11**: 2065 (1978). https://doi.org/10.1088/0022-3719/11/10/017
33. S.E. Lindgren and L. Walldén, *Solid State Commun.*, **28**: 283 (1978). https://doi.org/10.1016/0038-1098(78)90644-0
34. S.E. Lindgren and L. Walldén, *Solid State Commun.*, **34**: 671 (1980). https://doi.org/10.1016/0038-1098(80)90952-7

35. S.D. Kevan and W. Eberhardt, *Angle-Resolved Photoemission. Theory and Current Applications* (Ed. S. D. Kevan) (Amsterdam: Elsevier: 1992), p. 99; idem, *Studies in Surface Science and Catalysis*, **74**: 99 (1992). https://doi.org/10.1016/S0167-2991(08)61774-7
36. F. Patthey and W.-D. Schneider, *Surf. Sci. Lett.*, **334**: L715 (1995); T.C. Hsieh and T.-C. Chiang, *Surf. Sci.*, **166**: 554 (1986). https://doi.org/10.1016/0039-6028(95)80022-0, https://doi.org/10.1016/0039-6028(86)90696-5
37. T.C. Hsieh, T. Miller, and T.-C. Chiang, *Phys. Rev. Lett.*, **55**: 2483 (1985).
38. D. Aburano, H. Hong, J. M. Roesler, K. Chung, D.-S. Lin, P. Zschak, H. Chen, and T.-C. Chiang, *Phys. Rev. B*, **52**: 1839 (1995). https://doi.org/10.1103/PhysRevB.52.1839
39. R. Abermann, *Vacuum*, **41**: 1279 (1990); R. Koch, D. Winau, A. Führmann, and K.H. Rieder, *Phys. Rev. B*, **44**: 3369 (1991); R. Koch, D. Winau, K. Thümer, M. Weber, and K.H. Rieder, *Europhys. Lett.*, **21**: 213 (1993). https://doi.org/10.1016/0042-207X(90)93933-A, https://doi.org/10.1103/PhysRevB.44.3369, https://doi.org/10.1209/0295-5075/21/2/016
40. C.Y. Fong and M.L. Cohen, *Phys. Rev. Lett.*, **24**: 306 (1970); C.Y. Fong, J.P. Walter, and M.L. Cohen, *Phys. Rev. B*, **11**: 2759 (1975). https://doi.org/10.1103/PhysRevLett.24.306, https://doi.org/10.1103/PhysRevB.11.2759
41. R.C. Jaklevic and J. Lambe, *Phys. Rev. B*, **12**: 4146 (1975). https://doi.org/10.1103/PhysRevB.12.4146
42. Gmelin Handbuch der Anorganischen Chemie, **A-Z/8** (Ed.R. Warncke) (Berlin–Heidelberg: Springer-Verlag: 1978). https://doi.org/10.1007/978-3-662-06224-1
43. G. Larsson and J.B. Pendry, *J. Phys. C*, **14**: 3089 (1981). https://doi.org/10.1088/0022-3719/14/21/025
44. C.-S. Jiang, H.-B. Yu, X.-D. Wang, C.-K. Shih, and Ph. Ebert, *Phys. Rev. B*, **64**: 235410 (2001). https://doi.org/10.1103/PhysRevB.64.235410
45. R.M. Feenstra, *J. Vac. Sci. Technol. B*, **7**: 925 (1989); P. Martensson and R.M. Feenstra, *Phys. Rev. B*, **39**: 7744 (1989); C.K. Shih, R.M. Feenstra, and G.V. Chandrashekhar, *Phys.Rev.B*, **43**: 7913 (1991). https://doi.org/10.1116/1.584582, https://doi.org/10.1103/PhysRevB.39.7744, https://doi.org/10.1103/PhysRevB.43.7913
46. N.E. Christensen, *Phys. Rev. B*, **20**: 3205 (1979). https://doi.org/10.1103/PhysRevB.20.320
47. K.-J. Chao, Zhenyu Zhang, Ph. Ebert, and C.-K. Shih, *Phys. Rev. B*, **60**: 4988 (1999). https://doi.org/10.1103/PhysRevB.60.4988
48. G. Neuhold, L. Bartels, J.J. Paggel, and K. Horn, *Surf. Sci.*, **376**: 1 (1997). https://doi.org/10.1016/S0039-6028(96)01393-3
49. Ph. Ebert, K.-J. Chao, Q. Niu, and C.-K. Shih, *Phys. Rev. Lett.*, **83**: 3222 (1999). https://doi.org/10.1103/PhysRevLett.83.3222
50. A.-B. Chen and B. Segall, *Phys. Rev. B*, **12**: 600 (1975). https://doi.org/10.1103/PhysRevB.12.600
51. K. Sawa, Y. Aoki, and H. Hirayama, *Phys. Rev. B*, **80**: 035428 (2009). https://doi.org/10.1103/PhysRevB.80.035428
52. K. He, T. Hirahara, T. Okuda, S. Hasegawa, A. Kakizaki, and I. Matsuda, *Phys. Rev. Lett.*, **101**: 107604 (2008). https://doi.org/10.1103/PhysRevLett.101.107604
53. H. Ibach, *Surf. Sci. Rep.*, **29**: 195 (1997). https://doi.org/10.1016/S0167-5729-(97)00010-1
54. M. Miyazaki and H. Hirayama, *Surf. Sci.*, **602**: 276 (2008). https://doi.org/10.1016/j.susc.2007.10.02

55. P. Mikulík, *Beyond Quasicrystals* (Eds. F. Axel and D. Gratias) (Berlin–Heidelberg: Springer-Verlag: 1995), p. 229. https://doi.org/10.1007/978-3-662-03130-8
56. M. Feuerbacher, C. Metzmacher, M. Wollgarten, K. Urban, B. Baufeld, M. Bartsch, and U. Messerschmidt, *Mater. Sci. Eng. A*, **226–228**: 943 (1997); R. Wang, M. Feuerbacher, W. Yang, and K. Urban, *Philos. Mag. A*, **78**: 273 (1998). https://doi.org/10.1016/S0921-5093(97)80097-4, https://doi.org/10.1080/01418619808241904
57. R. Mikulla, P. Gumbsch, and H.-R. Trebin, *Philos. Mag. Lett.*, **78**: 369 (1998); R. Mikulla, J. Stadler, F. Krul, H.-R. Trebin, and P. Gumbsch, *Phys. Rev. Lett.*, **81**: 3163 (1998). https://doi.org/10.1080/095008398177760, https://doi.org/10.1103/PhysRevLett.81.3163
58. V.L. Karbivskyy, V.V. Vishniak, V.H. Kasiyanenko, *J. Adv. Microsc. Res.* **6**: 278 (2011). https://doi.org/10.1166/jamr.2011.1083
59. V. Karbivskyy, L. Karbivska, and V. Artemyuk, *Nanoscale Res. Lett.*, **11**: 69 (2016). https://doi.org/10.1186/s11671-016-1291-2
60. V.A. Artemyuk, L.I. Karbivska, O.Ya. Kuznetsova, V.L. Karbivskyy, L.P. Klyuyenko, and S.S. Smolyak, *Usp. Fiz. Met.*, **18**, No. 3: 235 (2017) (in Ukrainian). https://doi.org/10.15407/ufm.18.03.235
61. L.I. Karbivska, O.Ya. Kuznetsova, V.L. Karbivskyy, S.S. Smolyak, and V.A. Artemyuk, *Usp. Fiz. Met.*, **20**, No. 1: 52 (2019) (in Russian). https://doi.org/10.15407/ufm.20.01.052

Received May 5, 2019;
in final version, July 30, 2019

Л.І. Карбівська, В.Л. Карбівський, А.О. Романський
Інститут металофізики ім. Г.В. Курдюмова НАН України,
бульв. Академіка Вернадського, 36, 03142 Київ, Україна

ДЕТЕРМІНІЗМ СИМЕТРІЇ МОНОКРИСТАЛІЧНОЇ ПОВЕРХНІ МЕЖІ ПОДІЛУ ПРИ ОДЕРЖАННІ 0*D*- І 2*D*-СТРУКТУР ШЛЯХЕТНИХ МЕТАЛІВ ТА ІНДІЮ НА КРЕМНІЇ

Оглядову статтю присвячено «квантовій інженерії» вирощування плівок срібла на напівпровідникових підкладинках, яке уможливлює одержання нових форм речовини. Наведено результати з енергетичної дисперсії електронних станів у епітаксіальних плівках Ag(111), одержаних на Si(001) та Si(111). Пояснено розщеплення зон і надано аналіз поверхневих станів за Шоклі. Детально аналізуються надструктури, які утворюються на поверхні моношарових наноструктур срібла. Наведено детальний аналіз енергетичних станів квантових ям шляхетних металів. Досліджено механізм формування нанорельєфу шляхетного металу на поверхнях (111) і (110) монокристалу Si при багатостадійному термічному напорошенні. Симетрія поверхні інтерфейсу монокристалічної площини кремнію Si(111) 7×7 є детермінувальною у механізмі росту гексагонально-пірамідальних структур міді, срібла та золота. Досліджено морфологічні особливості поверхні індію при його термічному нанесенні на поверхні Si(111) і Si(110). Спостерігається утворення кластерів правильної кубічної форми, що свідчить про формування нанокристалів In. Утворення нанокластерів In (розміром у ≈10 нм) на поверхні Si(111) і подальше змінення морфології поверхні монокристалу модифікують розраховані криві густини електронних станів.

Ключові слова: квантові ями, енергетична дисперсія, шляхетні метали, поверхня, морфологія, сканувальна тунельна мікроскопія, термічне напорошення.

Л.И. Карбовская, В.Л. Карбовский, А.А. Романский
Институт металлофизики им. Г.В. Курдюмова НАН Украины,
бульв. Академика Вернадского, 36, 03142 Киев, Украина

ДЕТЕРМИНИЗМ СИММЕТРИИ МОНОКРИСТАЛЛИЧЕСКОЙ ПОВЕРХНОСТИ ГРАНИЦЫ РАЗДЕЛА ПРИ ПОЛУЧЕНИИ 0*D*- И 2*D*-СТРУКТУР БЛАГОРОДНЫХ МЕТАЛЛОВ И ИНДИЯ НА КРЕМНИИ

Обзорная статья посвящена «квантовой инженерии» выращивания плёнок серебра на полупроводниковых подложках, которое позволяет получать новые формы вещества. Приведены результаты по энергетической дисперсии электронных состояний в эпитаксиальных плёнках Ag(111), полученных на Si(001) и Si(111). Объяснено расщепление зон и дан анализ поверхностных состояний Шокли. Детально анализируются сверхструктуры, которые образуются на поверхности монослойных наноструктур серебра. Приведён детальный анализ энергетических состояний квантовых ям благородных металлов. Исследован механизм формирования нанорельефа благородного металла на поверхностях (111) и (110) монокристалла Si при многостадийном термическом напылении. Симметрия поверхности интерфейса монокристаллической плоскости кремния Si(111) 7×7 является детерминирующей в механизме роста гексагонально-пирамидальных структур меди, серебра и золота. Исследованы морфологические особенности поверхности индия при его термическом нанесении на поверхности Si(111) и Si(110). Наблюдается образование кластеров правильной кубической формы, что свидетельствует о формировании нанокристаллов In. Образование нанокластеров In (размером $\approx$10 нм) на поверхности Si(111) и дальнейшее изменение морфологии поверхности монокристалла модифицируют рассчитанные кривые плотности электронных состояний.

Ключевые слова: квантовые ямы, энергетическая дисперсия, благородные металлы, поверхность, морфология, сканирующая туннельная микроскопия, термическое напыление.